J|A|C|S ARTICLES

Published on Web 01/05/2009

From Monomer to Bulk: Appearance of the Structural Motif of Solid Iodine in Small Clusters

Eero Hulkko, Toni Kiljunen,* Tiina Kiviniemi, and Mika Pettersson

Nanoscience Center, Department of Chemistry, P.O. Box 35, FI−40014 University of Jyväskylä, Finland

Received August 18, 2008; E-mail: toni.k.kiljunen@jyu.fi

Abstract: Formation of iodine clusters in a solid krypton matrix was studied using resonance Raman spectroscopy with a 1 cm^{-1} resolution. The clusters were produced by annealing of the solid and recognized by appearance of additional spectral transitions. Two distinct regions, red-shifted from the fundamental vibrational wavenumber of the isolated I_2 at 211 cm^{-1}, were observed in the signal. The intermediate region spans the range 196−208 cm^{-1}, and the ultimate region consists of two peaks at 181 and 190 cm^{-1} nearly identical to crystalline I_2. The experimental results were compared to DFT-D level electronic structure calculations of planar $(I_2)_n$ clusters ($n = 1-7$). The dimer, trimer, and tetramer structures, where the I_2 molecule is complexed from one end, were found to exhibit vibrational shifts corresponding to the intermediate size clusters. The larger, bulklike shift appears when the iodine molecule is coordinated from two opposite directions as in the case of a pentamer and higher clusters. Starting from the pentamer, the structural motif of crystalline iodine is clearly recognized in the clusters.

Introduction

Iodine is an element with many fascinating properties. The solid phase has a layered structure where I_2 molecules within a layer are ordered in a zigzag pattern.[1] Besides the electron pair repulsion and dispersive attraction, multipolar and charge-transfer effects manifest themselves in the dense packing of the molecular solid. The shortest interatomic distance within a layer is 3.50 Å, and the corresponding distance between the layers is 4.27 Å.[1] The interatomic distance in molecular I_2 is somewhat longer in the solid state (2.715 Å)[1] than in the isolated molecule (2.666 Å).[2] Solid iodine can be considered as a two-dimensional semiconductor with a much higher conductivity in the layer plane than perpendicular to it.[3] It becomes metallic at 16 GPa and shows a molecular to monatomic transition at 21 GPa.[4−6] Several other high-pressure phases have been found, and this field is of high current interest.[7] The structure of liquid iodine has also received considerable attention. X-ray diffraction studies have indicated a short-range orientational order suggesting that the structure of a layer in the solid state is partially preserved in molten iodine.[8] The bond length of I_2 in liquid (2.70 Å)[8] is intermediate between the solid and gas phase values.

Raman spectroscopy has been particularly informative in the studies of different phases of iodine. In the solid phase, two stretching modes are observed for I_2 at 180 and 189 cm^{-1} with symmetries A_g and B_{3g}, respectively.[9] There are two molecules of I_2 in the unit cell, and the two vibrations can be considered as in-phase (180 cm^{-1}) and out-of-phase (189 cm^{-1}) modes. In the liquid phase, the main Raman peak is observed at 194 cm^{-1}, and it moves to higher wavenumbers, up to ∼205 cm^{-1}, at lower densities.[10,11] Interestingly, the position of the peak is in between the values for solid and gaseous iodine. Another broad signal at 175−185 cm^{-1} was assigned to small clusters of iodine, $(I_2)_n$. Additionally, ionic species were observed as evidenced by the 110 cm^{-1} Raman peak associated with I_3^-.[10]

In view of the long history of investigations of the properties of iodine, it is surprising how little is known about the dimer and other small clusters. This situation especially concerns neutral iodine since, for negative ions, vast literature exists and polyiodide species up to I_{29}^{3-} have been characterized.[12] The formation enthalpy of the neutral iodine dimer was determined from the gas phase UV absorption by Passchier and Gregory who obtained a value of -12 ± 2 kJ/mol at 605 K.[13] The only Raman data on isolated aggregates seems to be the matrix isolation study of Howard and Andrews who assigned the observed 180 cm^{-1} peak to small aggregates $(I_2)_n$ with $n = 2-4$.[14] Later, the same peak was observed in free-standing crystals of rare gases by Almy et al. who assigned it to dimers.[15] It is worth noting that, in the above studies, the used instrumental

(1) van Bolhuis, F.; Koster, P. B.; Migchelsen, T. *Acta Crystallogr.* **1967**, *23*, 90–91.
(2) Huber, K. P.; Herzberg, G. *Constants of Diatomic Molecules*; Van Nostrand Reinhold: New York, 1979.
(3) Greenwood, N. N.; Earnshaw, A. *Chemistry of the Elements*, 2nd ed.; Elsevier: Amsterdam, 2006.
(4) Balchan, A. S.; Drickamer, H. G. *J. Chem. Phys.* **1961**, *34*, 1948–1949.
(5) Takemura, K.; Fujii, Y.; Minomura, S.; Shimomura, O. *Solid State Commun.* **1979**, *30*, 137–139.
(6) Fujii, Y.; K.; Hase, N. H.; Ohishi, Y.; Onodera, A.; Shimomura, O.; Takemura, K. *Phys. Rev. Lett.* **1987**, *58*, 796–799.
(7) Zeng, Q.; He, Z.; San, X.; Ma, Y.; Tian, F.; Cui, T.; Liu, B.; Zou, G.; Mao, H.-k. *Proc. Natl. Acad. Sci. U.S.A.* **2008**, *105*, 4999–5001.
(8) van der Marel, C.; Bras, W.; van der Lugt, W. *Mol. Phys.* **1988**, *64*, 445–456.
(9) Congeduti, A.; Nardone, M.; Postorino, P. *Chem. Phys.* **2000**, *256*, 117–123.
(10) Magana, R. J.; Lannin, J. S. *Phys. Rev. B* **1985**, *32*, 3819–3823.
(11) Magana, J. R.; Lannin, J. S. *Phys. Rev. B* **1988**, *37*, 2475–2483.
(12) Svensson, P. H.; Kloo, L. *Chem. Rev.* **2003**, *103*, 1649–1684.
(13) Passchier, A. A.; Gregory, N. W. *J. Phys. Chem.* **1968**, *72*, 2697–2702.
(14) Howard, W. F., Jr.; Andrews, L. *J. Raman. Spect.* **1974**, *2*, 447–462.

10.1021/ja806537u CCC: $40.75

resolution was on the order of 10 cm^{-1} which is far from optimal for resolving signals due to clusters of various size.

Iodine is increasingly being used in novel geometries in nanoscopic systems. An important breakthrough in TiO_2 based photocatalyst was recently achieved by introducing iodine molecules during fabrication of a nanovoid-structured TiO_2 material.[16] The encapsulated, thermally stable $(I_2)_n$ adducts on the cavity walls act as light harvesting antennas to create excitons transferred to the catalytic reaction zone, and thereby significantly enhance the TiO_2 photoactivity. Robust evidence for the presence of $(I_2)_n$ aggregates inside the voids was obtained by Raman spectroscopy showing the 179 cm^{-1} mode. In a recent study, one-dimensional wires of molecular iodine were fabricated inside zeolite channels.[17] In these samples, the observed Raman peak at 110 cm^{-1} was assigned to I_3^-, and the peak at 168 cm^{-1} was attributed to $(I_2)_n$ wires without specifying the order of n. As yet another surprise, as far as we know, virtually no electronic structure calculations exist for small clusters of iodine. Clearly, there is high need for experimental and computational studies aimed at elucidating properties of the dimer and small clusters of iodine since they bridge the gap between the monomer and the bulk and help to understand the appearance of bulk properties and to assign observed Raman bands to correct species in various samples.

In this paper, we report Raman spectroscopic observations and electronic structure calculations of iodine dimer and clusters $(I_2)_n$ up to $n = 7$. The complexes are produced in a low-temperature krypton matrix where Raman bands are intrinsically narrow and, combined with sufficiently high instrumental resolution, allow distinguishing several complexes in the experimental spectra. The electronic structure calculations help to assign the experimentally observed features, and both methods together yield a consistent picture of the appearance of the structural motif of bulk solid iodine already in the pentaiodine cluster. Simultaneously, the Raman spectrum shifts systematically from the monomer value toward the characteristic spectrum of the bulk. In qualitative terms, the shift is in fact a two-stage process, where the first stage corresponds to intermediate clusters and the second stage manifests the structural motif prevailing in bulk solid. These results help us to understand the Raman spectrum of iodine in various forms ranging from liquid and amorphous phases to novel geometries such as molecular wires and nanoclusters.

Methods

Experimental Section.

Gaseous impurities were removed from a solid iodine sample by performing several freeze−pump−thaw cycles. Krypton gas was used without further purification (99.997%). Gas mixture at 1:2600 I_2:Kr ratio was prepared to a 5 dm^3 glass bulb at room temperature. As described in detail previously,[18] solid matrix samples were prepared by continuous, slow deposition of the premixed gas onto a cold substrate (100 μm thick sapphire window) mounted on a helium flow cryostat kept at 40 K temperature. After the deposition, the sample was slowly cooled to 32 K. The Stokes branch resonance Raman spectra were measured using a 532 nm single-mode frequency-doubled CW Nd:YAG laser (Alphalas). The 532 nm laser line was chosen for efficient resonance enhancement by exciting at the maximum of the broad $B^3\Pi_{0u} \leftarrow X^1\Sigma_{0g}$ transition band of the I_2 molecule in Kr.[18] The overlapping $^1\Pi_{1u} \leftarrow X^1\Sigma_{0g}$ transition[19] further supports the resonance enhancement. The Raman spectra were recorded during an annealing process that elevated the cryostat temperature from 32 to 86 K at a 1 K/min rate. The laser power was kept at 2 mW (ca. 1 W/cm^2) in order to minimize local heating of the sample. The spectra were collected in a back-scattering configuration using a 50 cm focal length spectrograph (Acton SpectraPro 2500i) with a 2400 groove/mm holographic grating. Peltier-cooled CCD detector (Andor Newton) was operated with 1 min/spectrum measurement time including six accumulations. The Rayleigh line of the laser was suppressed by an edge filter (Semrock). The resolution of the measured Raman spectra was 1 cm^{-1} as determined from the instrument-limited line width of the $v = 1$ band of the I_2 molecule. The wavenumber scale of the Raman spectra was calibrated at 32 K from the Raman peaks of monomeric I_2 using the Morse potential parameters $\tilde{\nu}_e = 211.20$ cm^{-1} and $\tilde{\nu}_e x_e = 0.642$ cm^{-1}, which were determined accurately for similarly prepared matrices by time-resolved coherent anti-Stokes Raman scattering spectroscopy (TR-CARS).[18]

Computational Section.

Density functional theory as implemented[20] in the TURBOMOLE V5.10 program package[21] was used for optimizing the I_2 cluster geometries[22] and computing the vibrational wavenumbers and Raman intensities.[23,24] On the basis of a set of test calculations performed for dimer structures,[25] the B3LYP parametrization was chosen for the exchange-correlation functional, and the empirical dispersive energy correction (DFT-D)[26] was used throughout. The scalar-relativistic pseudopotential ECP46MWB[27] was used together with a polarized triple-ζ valence (TZVPP)[28] basis set that has been reported to provide a reasonable overall description of the Raman spectrum.[24] A 514.5 nm laser wavelength was used in the formula that yields the nonresonant Raman cross sections. Natural population analysis and electrostatic potential calculations were carried out for evaluating the charge distributions.[29] A set of ab initio MP2 calculations (details given in Supporting Information) for the cluster structures and spectra was also performed in order to further validate the results obtained by the DFT-D.

(15) Almy, J.; Kizer, K.; Zadoyan, R.; Apkarian, V. A. *J. Phys. Chem. A* **2000**, *104*, 3508–3520.
(16) Usseglio, S.; Damin, A.; Scarano, D.; Bordiga, S.; Zecchina, A.; Lamberti, C. *J. Am. Chem. Soc.* **2007**, *129*, 2822–2828.
(17) Ye, J. T.; Tang, Z. K.; Siu, G. G. *Appl. Phys. Lett.* **2006**, *88*, 073114.
(18) Kiviniemi, T.; Aumanen, J.; Myllyperkiö, P.; Apkarian, V. A.; Pettersson, M. *J. Chem. Phys.* **2005**, *123*, 064509.
(19) Gray, R. I.; Luckett, K. M.; Tellinghuisen, J. *J. Phys. Chem. A* **2001**, *105*, 11183–11191.
(20) Treutler, O.; Ahlrichs, R. *J. Chem. Phys.* **1995**, *102*, 346.
(21) Ahlrichs, R.; Bär, M.; Häser, M.; Horn, H.; Kölmel, C. *Chem. Phys. Lett.* **1989**, *162*, 165.
(22) von Arnim, M.; Ahlrichs, R. *J. Chem. Phys.* **1998**, *111*, 9183.
(23) Delgmann, P.; Furche, F.; Ahlrichs, R. *Chem. Phys. Lett.* **2002**, *362*, 511.
(24) Rappoport, D.; Furche, F. *J. Chem. Phys.* **2007**, *126*, 201104.
(25) The functionals PB86, PBE, PBE0, B97D, and B3LYP were used for geometry optimization and vibrational wavenumbers of the I_2 dimer, and compared to results obtained with separate MP2-level ab initio calculations. The MP2 methods were RI-MP2/TZVPP in the Turbomole and MP2/aug-cc-pVTZ in the Molpro suite of programs, where BSSE correction was also performed. The proper "L-shape" structure was obtained with the B97D and B3LYP+D functionals, and the latter suits better for vibrational wavenumber evaluations.
(26) Grimme, S. *J. Comput. Chem.* **2006**, *27*, 1787–1799.
(27) Bergner, A.; Dolg, M.; Küchle, W.; Stoll, H.; Preuss, H. *Mol. Phys.* **1993**, *80*, 1431.
(28) Weigend, F.; Häser, M.; Patzelt, H.; Ahlrichs, R. *Chem. Phys. Lett.* **1998**, *294*, 143.
(29) Martin, F.; Zipse, H. *J. Comput. Chem.* **2004**, *26*, 97–105.

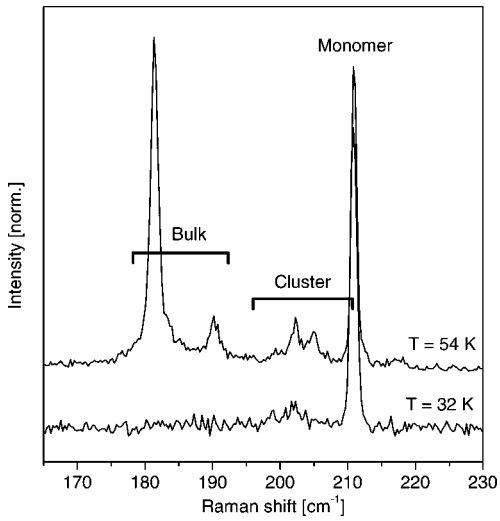

Figure 1. Resonance Raman spectra obtained at 32 K after the deposition of the 1:2600 I_2:Kr gas mixture (lower spectrum) and at 54 K after the 1 K/min rate annealing of the sample (upper spectrum). The spectrum from the annealed sample (normalized to the 211 cm^{-1} peak height) shows three distinct regions assigned to monomer, cluster, and bulklike contributions.

Results

Experimental Findings from Monomers to Bulk. Solid Kr provides a weakly perturbing environment for studying isolated I_2 molecules and small molecular aggregates. The fundamental vibrational wavenumber manifests the small matrix effect by the 3−4 cm^{-1} red shift[14,18,30] from the $\tilde{\nu}_e$ = 214.5 cm^{-1} gas phase value.[2,31] Almost completely monomeric trapping of I_2 in solid Kr can be obtained by the slow deposition of the dilute gas mixtures at 40 K. This can be seen in Figure 1, where the lower Raman spectrum is recorded at 32 K directly after the deposition and cooling. The presence of an isolated I_2 is identified from the distinct Raman band at 211 cm^{-1} (210.8 cm^{-1}).

The upper Raman spectrum in Figure 1 summarizes the experimental results observed for the $v = 1$ band of iodine by showing the spectral changes arising upon annealing of the sample. The 54 K temperature chosen for the presentation, i.e., after 22 min of heating, contains three distinct features in the proximity of the fundamental vibration of iodine. In addition to the 211 cm^{-1} peak, a broader signal consisting of a set of peaks appears further red-shifted. Finally, a doublet signal exhibiting the vibrational wavenumbers of solid I_2 is formed as the ultimate feature in the spectra. We nominate the three regions as monomer, cluster, and bulklike features according to the assumed origins of the signals as will be discussed below.

The top panel in Figure 2 represents a series of spectra taken during the annealing process. The series is initiated after recording the lower spectrum (T = 32 K) in Figure 1 and optimizing the signal. Consequently, the first spectrum at T = 33 K already shows signal intensity in the cluster region due to laser heating of the sample. Ultimately, the annealing leads to a dramatic change in the Raman spectrum, when the two bands at 181 cm^{-1} (181.4 cm^{-1}, 60 K) and 190 cm^{-1} (190.3 cm^{-1}) begin to dominate the signal at the 52−53 K temperature. These

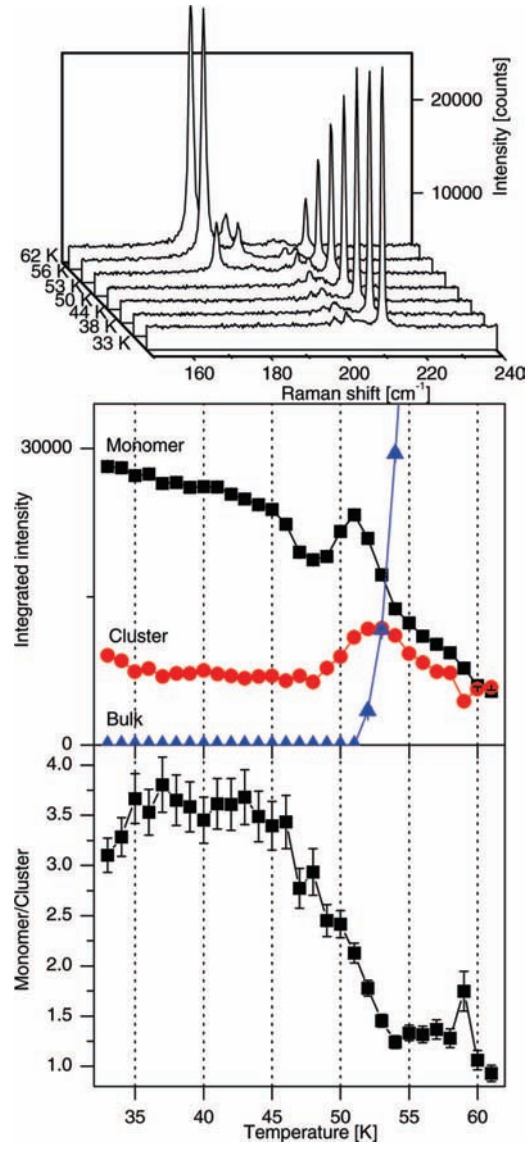

Figure 2. Temperature dependence of the resonance Raman spectrum. Top: Annealing of the sample from 32 to 62 K. Middle: Integrated intensities of the decaying monomer (212 cm^{-1}) and cluster (194−207 cm^{-1}) signals and the sudden rise of the bulk signal (181 cm^{-1}). Bottom: The signal ratio from the I_2 and $(I_2)_n$ contributions.

wavenumbers are nearly identical to the two strongly Raman-active lattice modes A_g and B_{3g} observed in crystalline I_2 [9,32] and indicate a formation of a solidlike I_2 species.

The crystalline I_2 lattice belongs to the orthorhombic *Cmca* space group (D_{2h}^{18}) symmetry.[1,33] The two observed Raman bands are the fundamental transitions of in-phase (180 cm^{-1}) and out-of-phase vibrations (189 cm^{-1}) of the two I_2 molecules in the primitive cell.[9,34]

Analysis of the Spectral Components. The spectral peak patterns from the different regions show a temperature dependence which is analyzed further in Figure 2. The middle panel shows the intensities of the monomer and bulk peaks and the cluster region during the annealing process. Integrated intensities

(30) Karavitis, M.; Kumada, T.; Goldschleger, I. U.; Apkarian, V. A. *Phys. Chem. Chem. Phys.* **2005**, *7*, 791–796.
(31) Holzer, W.; Murphy, W. F.; Bernstein, H. J. *J. Chem. Phys.* **1970**, *52*, 399–407.
(32) Anderson, A.; Sun, T. S. *Chem. Phys. Lett.* **1970**, *6*, 611–616.
(33) Ibberson, R. M.; Moze, O.; Petrillo, C. *Mol. Phys.* **1992**, *76*, 395–403.
(34) Congeduti, A.; Postorino, P.; Nardone, M.; Buontempo, U. *Phys. Rev. B* **2001**, *65*, 014302.

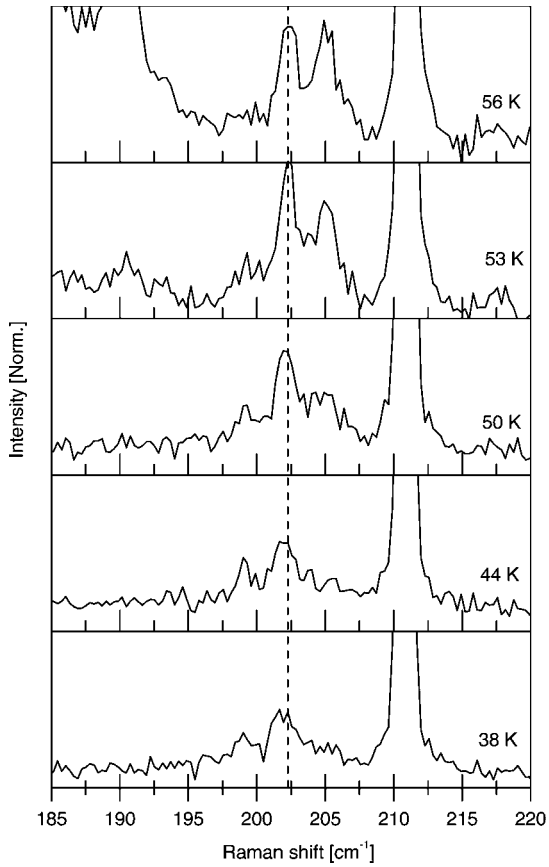

Figure 3. Temperature dependence of the resonance Raman spectra emphasized for the intermediate region at 198−208 cm^{-1}. The dashed line is added to locate the most abundant cluster contribution at 202 cm^{-1}.

of the monomer and bulk contributions were obtained by fitting the 211 and 181 cm^{-1} peaks with a single Gaussian function. The cluster contributions were obtained by integrating the band area in the 194−207 cm^{-1} region. The curves thus obtained represent the onset of a molecular mobilization in Kr by the coincidence of the bulk signal rise with the decay of the monomer and aggregate signals. The transient positive kinks of the decaying signals between 50 and 55 K probably result from modification of the optical properties of the sample upon softening of the solid structure.

Because of the difficulty in fitting the cluster region to well resolved, separate contributions, the total intensity of the area is presented with respect to the monomer signal in the lowest panel of Figure 2. The monomer and cluster intensities show a steady decrease in the temperature interval $T = 33-45$ K while the signal ratio remains approximately the same. The initial kinetics is partially masked due to the intermediates produced by the laser heating. The mobilized monomers begin to feed the cluster region in the $T = 45-50$ K interval where no sign of the bulklike signal is yet formed. The relative intensity continues to change steadily until 55 K is reached where the bulk contribution takes over the signal.

Figure 3 emphasizes the intermediate region of the spectra. The new features appearing in the 198−208 cm^{-1} range reveal subtle changes during the annealing from 32 K. Several Raman bands overlap in this region with a varying intensity pattern. The most intense peak is located at 202 cm^{-1}, until at 56 K it is accompanied by an equally intense peak at 205 cm^{-1}. At the same time, the neighboring peak at 199 cm^{-1} fades. Qualitatively, at least these three local maxima are resolved which

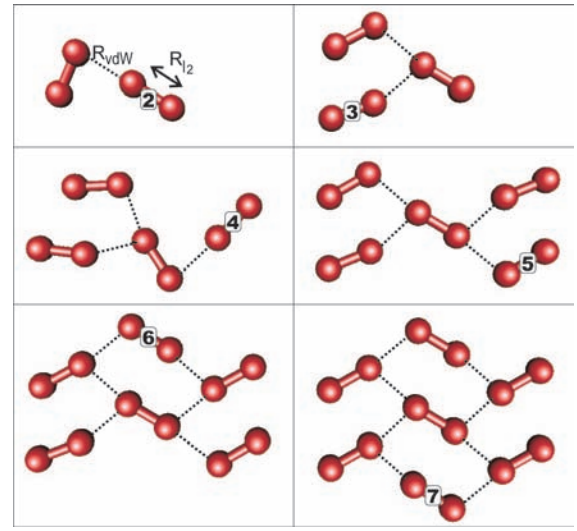

Figure 4. Planar $(I_2)_{2-7}$ cluster geometries optimized at the DFT-D/B3LYP/TZVPP level. Each panel is labeled by the additional molecule attached to the smaller structure. Shortest intermolecular distances R_{vdW} are indicated by dotted lines, while R_{I_2} is reserved for the bond length at the central molecule. The horizontal and vertical grid lines correspond to lattice axis directions c and b of the solid iodine, respectively.

correspond to as many different species based on the changing relative intensities. In addition, we note that the intense monomer signal overlaps with some cluster contributions as is indicated by the line-shape asymmetry which increases at higher temperatures.

Computational Evaluations. The bond length R_{I_2} of 2.702 Å obtained with the present computational method for the I_2 molecule is modified upon complexation. In the case of a dimer, an "L-shape" structure is formed (see Figure 4), and the bond length splits to 2.699 and 2.716 Å while the formed intermolecular atom-to-atom distance R_{vdW} (dotted line in Figure 4) is 3.805 Å in agreement with twice the van der Waals radius of 1.892 Å, which is used in the dispersive energy correction formula. The energy of a dimer formation is here calculated to be −13.56 kJ/mol. The contribution from the dispersive energy correction is −9.65 kJ/mol at this geometry, while a geometry optimization without the correction term gives a near "T-shape" structure and a −5.68 kJ/mol dimer formation energy. The elongated fragment, assigned by the number $n = 2$ in Figure 4, acquires negative partial charges δ^- according to the natural population analysis. The partial charges are $-0.034e$, $-0.012e$, $+0.027e$, and $+0.019e$ from right to left in the dimer panel of Figure 4, respectively.

All the clusters $(I_2)_n$ ($n = 2-7$) presented in Figure 4 are confined in the bc plane of a crystalline, normal pressure iodine. The presented trimer is the minimum energy structure among three isomers separated by 5−7 kJ/mol in total energy, while the tetramer has another planar isomer separated by 1.4 kJ/mol. We note that for $n \geq 4$ small imaginary wavenumbers (<10i cm^{-1}) appear that correspond to out-of-plane bending modes. Reoptimizations from distorted C_1 structures always restored the planar (C_s) structures. The crystal plane structure begins to emerge at $n = 5$ where the pentamer assumes a C_{2h} symmetry. In terms of the crystal structure, molecules 3, 4, and 5 are just replicas of the first I_2 unit, and the pair 1−2 comprises a unit shell. The central molecule has a 2-fold coordination from both ends of the bond now. In the case of hexamers, four starting geometries were used. Two of them were planar such that the sixth molecule was separated by the lattice constant b (vertically)

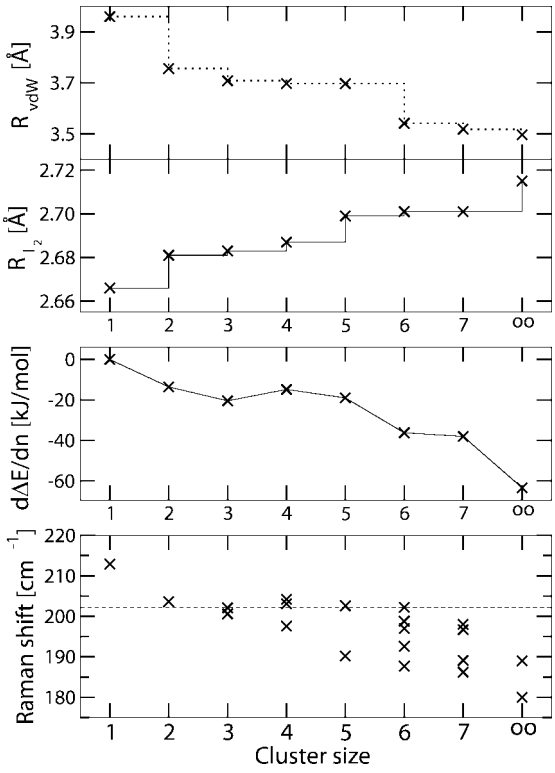

Figure 5. Compilation of computed properties as a function of the cluster size n representing the changes from a monomer to a bulk solid ($n = \infty$). Top panel: The shortest intermolecular distance R_{vdW} and the I_2 bond length R_{I_2}. The computed values are scaled to the monomer gas phase value. Middle panel: Convergence of the cohesion energy. Bottom: Vibrational wavenumbers of the clusters. The dashed line at 202 cm^{-1} as in the Experimental Section part of the Methods section (Figure 3).

or c (horizontally) from the pentamer central molecule. The direction b was more attractive by 5.4 kJ/mol. Molecules added out-of-plane by half of the lattice constant $a = 7.18$ Å either converged back to the bc plane or were trapped in a high energy (14 kJ/mol) composition. The converged heptamer is again a C_{2h} symmetric structure, where the central molecule is now fully coordinated by the planar network of I_2 fragments. Partial charges for the heptamer exhibit a peculiar pattern, where the outermost six atoms, i.e., all the loose ends of the cluster, acquire a negative partial charge. Opposite to the dimer case, atoms of the elongated, central fragment are left with a positive partial charge.

The calculated distances are represented as the function of the cluster size n and scaled by the factor 2.666/2.702 (gas-phase/calculated monomer) in Figure 5. The upmost panel shows the shortest intermolecular atom-to-atom distance R_{vdW} present in a cluster (dotted line). The $n = \infty$ value 3.496 Å represents the shortest intermolecular distance found in a pure iodine crystal[1,35] while for the $n = 1$ case the van der Waals distance 3.96 Å[36,37] (that agrees with the minimum energy distance of the dispersion correction formula) is shown. The lower half of the top panel represents the change of the intramolecular distance for the central, most distorted molecule (see Figure 4) from the gas phase[2] 2.666 Å value to the bulk solid[1] value ($n = \infty$) of 2.715 Å.

The experimental enthalpy of formation for a $(I_2)_2$ dimer, $\Delta H = -12 \pm 2$ kJ/mol (at 605 K),[13] agrees with the present calculated value of −13.1 kJ/mol including the zero-point energy correction. Each molecule added to a smaller cluster increases the total binding energy

$$\Delta E(n) \equiv E_n - nE_1 \tag{1}$$

such that $|\Delta E(n)| > |\Delta E(n-1)|$. For the range of $n = 2 \rightarrow 7$, the ΔE changes from −13.6 to −142.1 kJ/mol, respectively. However, the differential change defined as

$$\frac{d\Delta E}{dn} \equiv \frac{\Delta E(n) - \Delta E(n-1)}{dn} = E_n - E_{n-1} - E_1 \tag{2}$$

(with $dn = 1$) represents the adhesion energy of a single molecule which should reach a saturation point. The curve is presented in the middle panel of Figure 5 and compared to the lattice energy −63.5 kJ/mol of the solid iodine.[38] This convergence plot shows that 60% of the bulk cohesion energy is covered by the planar cluster structure.

The vibrational wavenumbers obtained by the analytical second derivatives of the converged DFT-D energy are shown in the lowest panel of Figure 5. The red shifts from the calculated monomer value of 212.9 cm^{-1} show two typical ranges; those shifted by ca. 10 cm^{-1} and those shifted by ca. 20 cm^{-1}. The stepwise shifting of the wavenumbers emerges from the complex formation. In the case of a dimer, the shifted mode (203.6 cm^{-1}) is localized to the elongated molecule with the negative partial charges. In a sense, the stretch vibration can be considered as hindered for one molecule (label 2 in Figure 4) while for the other molecule it is practically free, exhibiting a monomer wavenumber (213.5 cm^{-1}, which is no more plotted based on the negligible Raman cross section with respect to the shifted one). The trend continues in larger clusters. The trimer has two shifted modes closely separated for molecule labels 2 and 3 and a nonshifted mode for the first fragment (not shown due to low relative intensity). The shifted modes are coupled vibrations localized at the two molecules. For the tetramer the splitting within the shifted modes is larger than for the dimer and localized at different fragments. Pentamer structure is the first one where the second stage of shift appears. Now, the central molecule is complexed from both ends which also leads to a marked increase in the R_{I_2} value. Heptamer structure exhibits the lowest wavenumbers calculated along with the largest interaction energies. All the modes are red-shifted by more than 14 cm^{-1} for this geometry. Inspection of the normal modes shows that the lowest wavenumber is always localized to the central, here fully coordinated, molecule. It is interesting to note that the Raman-allowed (A_g) modes for the heptamer are grouped to oscillations where molecules 2 and 3 (comprising a bulk unit shell) are either in phase (186−189 cm^{-1}) or out of phase (197−198 cm^{-1}) with respect to each other. While the calculated absolute wavenumbers are still higher than the bulk values, the splitting resembles that of the bulk crystal's in-phase (180 cm^{-1}) and out-of-phase (189 cm^{-1}) modes shown at $n = \infty$.

Discussion

Partial Charge Delocalization. As known already from the X-ray and neutron diffraction crystal structure studies,[1,33] the iodine forms planes consisting of two-dimensional networks of nearly linear chains. The intermolecular separations shorter than the van der Waals distance and the elongated molecular bond lengths are manifestations of electron delocalization and inter-

(35) Kobashi, K.; Etters, R. D. *J. Chem. Phys.* **1983**, *79*, 3018–3025.
(36) Rowland, R. S.; Taylor, R. *J. Phys. Chem.* **1996**, *100*, 7384–7391.
(37) Bondi, A. *J. Phys. Chem.* **1964**, *68*, 441–451.
(38) English, C. A.; Venables, J. A. *Proc. R. Soc. London, Ser. A* **1974**, *340*, 57–80.

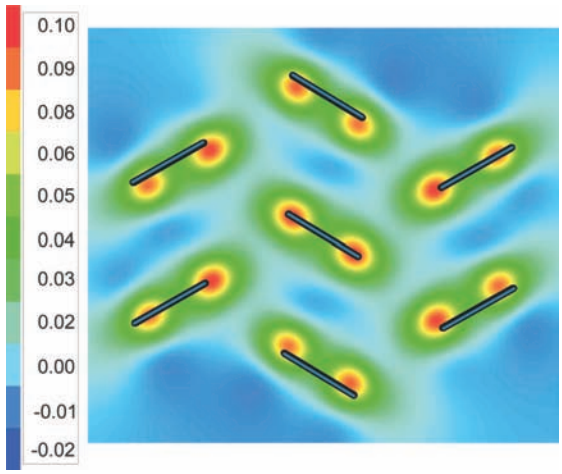

Figure 6. Electrostatic potential (in a.u.) for the calculated heptamer structure. The contour cut-plane is plotted 1.5 Å below the molecular plane (I_2 sticks) and highlights the inward shift of the positive partial charge from the positions of the nuclei thus leaving a negative outer shell surrounding the cluster.

molecular charge-transfer bonding. In order to visualize the situation, a contour plot of the charge distribution is shown in Figure 6 as a cut-plane of the electrostatic potential derived from the computed density for the heptamer structure. A negative partial charge cloud is found to surround the cluster, and as a result, the positive contribution appears drawn inward as illustrated in Figure 6.

Magana and Lannin[10] have searched for clustered molecules and ions in liquid iodine and state that the 180 cm^{-1} Raman band supports their interpretation of resonant enhancement from clusters of $(I_2)_n$. A solid state analogue to our study is reported in Allen and Comins' work,[39] where a γ-irradiated RbI exhibits a 201 cm^{-1} Raman band assigned to an I_2 molecule bound to a polar crystalline environment. Furthermore, increasing the temperature (from 233 K) resulted in molecular mobilization and a dominating 180 + 189 cm^{-1} doublet attributed to large $(I_2)_n$ aggregates. When an I_2 molecule becomes coordinated to an electron donor, the force constant is reduced and the vibrational mode moves to lower wavenumbers.[12] Buontempo et al.[40] tabulated the variation of I_2 bond lengths in gas, liquid, and solid phases as well as in solvents benzene, toluene, Et_2O, and EtOH. The range of 2.681−2.720 Å for R_{I_2} was obtained using the EXAFS spectroscopy.[40,41] The linear dependence of the Raman band red shift on the liquid density[11] and the corresponding exponential bond elongation as revealed by the EXAFS spectra[41] have been demonstrated. In our dimer example, the acceptor molecule acquires the partial negative charge and elongates as the donor molecule contracts. For the higher clusters, however, the bond length of the central molecule elongates despite the positive charge. For this limit, the bond elongation results from the charge delocalization and the intermolecular coupling within the binding network.

Two-Stage Shifting of Raman Bands. Figure 7 summarizes the calculated Raman bands. The cross sections span 2 orders of magnitude, the monomer peak being the weakest feature in

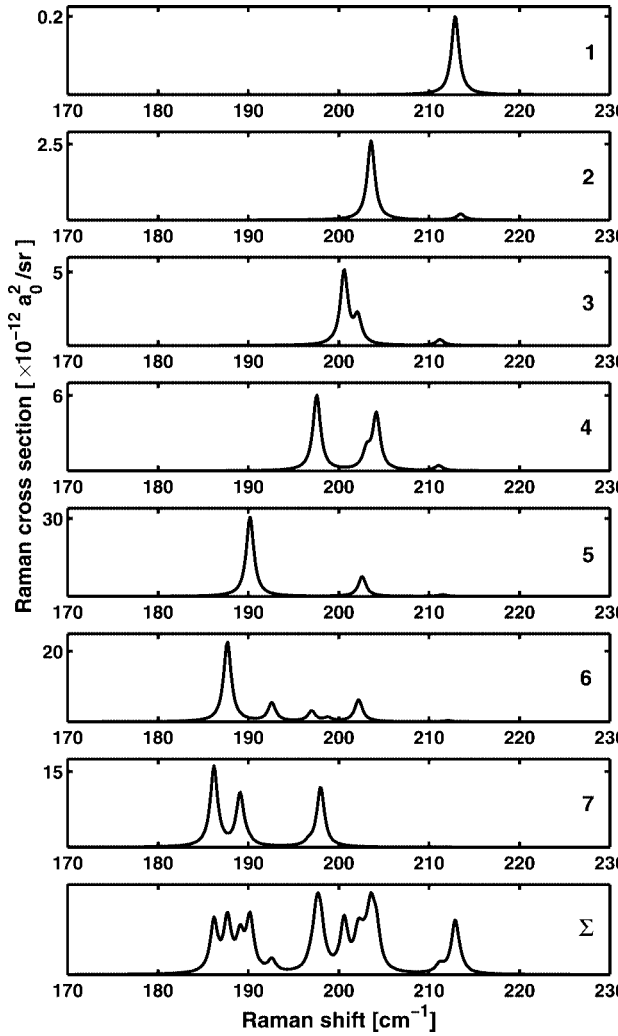

Figure 7. Raman bands calculated for the $(I_2)_n$ ($n = 1-7$) cluster structures represented by Lorentzian functions of 1 cm^{-1} width. As illustrated in the panel Σ where the signals are scaled and added together, the Raman shifts manifest three distinct wavenumber regions for the clusters: The monomeric contributions at $\tilde{\nu} > 210$ cm^{-1}, the intermediate region around 200 cm^{-1}, and the region for large clusters below 190 cm^{-1}.

the spectra. The intermediate region around 200 cm^{-1} with a notably higher intensity consists of several peaks belonging to small clusters. For the cluster sizes $n \geq 5$, a region of intense signal appears where the red shift from the monomer region is doubled as compared to the intermediate region. The charge redistribution discussed above shows up also in the increasing polarizability derivatives that are in the kernel of the intensity computation (quadratic dependence). The largest values and therefore intensities always correspond to the most red-shifted mode localized at the central fragment of a cluster. The two major scale changes, i.e., when going from monomer to dimer and from tetramer to pentamer, coincide with the wavenumber-shift stages. We note also that nonzero dipole moments 1.30 D, 0.91 D, 1.27 D, and 2.33 D arise for the less symmetric $n =$ 2, 3, 4, and 6 clusters, respectively. The intermediate region thus exhibits IR-active bands that do not show up in C_{2h} (A_g) symmetric pentamer and heptamer cases. The experimental signal intensities result (besides the number density) from the resonance condition, whereby the amount of enhancement can change from complex-to-complex in an irregular fashion. Therefore, merely to emphasize the emergence of the three

(39) Allen, A. M. T.; Comins, J. D. *J. Phys.: Condens. Matter* **1992**, *4*, 2701–2719.
(40) Buontempo, U.; Cicco, A. D.; Filipponi, A.; Nardone, M.; Postorino, P. *J. Chem. Phys.* **1997**, *107*, 5720–5726.
(41) Buontempo, U.; Filipponi, A.; Postorino, P.; Zaccari, R. *J. Chem. Phys.* **1998**, *108*, 4131–4137.

Table 1. Assignments and Predictions of the $(I_2)_n$ Aggregate Raman Bands in Kr[a]

aggregate	$\tilde{\nu}_{expt}$	$\Delta\tilde{\nu}_{expt}$	$\Delta\tilde{\nu}_{calcd}$
monomer	211		
dimer	202	− 9	− 9
trimer	199	− 12	− 11
			− 12
tetramer	205	− 6	− 9
			− 15
pentamer			− 10
			− 23
hexamer			− 25
heptamer			− 15
			− 24
			− 27
bulk	181	− 31	
	190	− 22	

[a] Listed are the observed resonance Raman shifts $\tilde{\nu}$ (in cm^{-1}) and their difference $\Delta\tilde{\nu}$ to the monomer value which are compared to those DFT-D calculated values that are most intense (see Figure 7). The first three clusters are distinguished in the resonance Raman spectra while the pentamer begins to overlap with the bulk contribution to the signal. The aggregates also exhibit unshifted contributions that overlap with the monomer signal.

distinct regions as found in the experiment, we construct an arbitrary sum spectrum by adding up the individual spectra after normalizing each by the highest peak intensity of that cluster. The outcome of the summation is labeled by Σ and shown in the lowest panel of Figure 7.

The division of the shifted vibrational wavenumbers into two groups can be approached from two directions. A cluster view explains the intermediate and large red shifts by two stages where the complex formation from one and both ends of a molecule takes place, respectively. The large red shift was reproduced also with higher-energy, chainlike trimer structures of the test calculations, where the central molecule was bound from both ends thus resembling a unit found in larger clusters and crystals. The bulk view, on the other hand, explains the two Raman bands as in-phase (A_g) and out-of-phase (B_{3g}) oscillations of the two molecules in the unit shell. Both of the viewpoints are applicable for the $n = 5-7$ size clusters, especially clearly for the C_{2h} symmetric pentamer and heptamer structures (A_g and B_{3g} representations of D_{2h} group correlate[42] with A_g in C_{2h}). In agreement with the bulk view, the intensity of the out-of-phase oscillation is lower than that for the in-phase mode. It can be anticipated that for even larger clusters the remaining splitting of the lowest mode (186−189 cm^{-1}) becomes merged and the red shifts reach the bulk wavenumbers relatively quickly.

To conclude the size n at which the 180 cm^{-1} bulk wavenumber appears in a DFT-D calculated $(I_2)_n$ spectrum, we give an order-of-magnitude accurate estimation of $n \sim 10^1$ based on the following. Heptamer is the first unit at which each molecular fragment is repeated at least twice. To remove the surface effect from the $n = 7$ unit, i.e., to bind the loose ends of that cluster, 10 additional in-plane surrounding molecules must be placed, thus significantly increasing the computational overhead. At the current level, the calculation gives by 27 and 24 cm^{-1} red-shifted values while the experiment shows 31 and 22 cm^{-1} values for the bulk shift (see Table 1). As the structural motif of bulk is formed in $n = 7$ nanocluster (area 1.4 nm^2), we consider the calculation sufficiently converged in order to proceed into the following assignments.

(42) Ferraro, J. R.; Nakamoto, K.; Brown, C. W. *Introductory Raman Spectroscopy*, 2nd ed.; Academic Press: San Diego, 2003.

Assignments. We assign the three peaks of the intermediate region (see Figure 3) to dimer, trimer, and tetramer contributions as listed in Table 1. The reasoning is based on the spectral abundance and temperature dependence as well as on the overall agreement with the theoretical results. Importantly, all the clusters scatter at intermediate wavenumbers between monomer and bulk. This allows the interpretation of the Raman spectra in different samples. In the work of Ye et al.,[17] the 168 cm^{-1} peak was assigned to neutral $(I_2)_n$ wires, but our results question this interpretation. An alternative assignment might be a higher polyiodide such as I_5^-, which has Raman signal in this region.[12] Usseglio et al.[16] used the 179 cm^{-1} resonance Raman band as complementary proof of $(I_2)_n$ doping of TiO_2 nanostructures without specifying the order of n. While their nanovoids (5−10 nm linear dimensions) can accommodate clusters up to $n \sim 10^3$, according to our results the size can range from a lower limit as small as $n \sim 10^1$. The liquid spectra, and especially the density dependence of the main Raman peak in the work of Magana and Lannin,[10,11] can be attributed to the decrease of the average coordination number of iodine molecules upon lowering the density.

Conclusion

The present experimental observation of Raman bands red-shifted in between the single molecule and crystalline phase limits brings the evidence for a formation of small $(I_2)_n$ aggregates in solid Kr. The monomeric (211 cm^{-1}), intermediate (198−208 cm^{-1}), and crystalline features (181 and 190 cm^{-1}) are all present at 54 K temperature. The peaks at 202, 199, and 205 cm^{-1} are assigned to the dimer, trimer, and tetramer, respectively. The corresponding monomer-to-complex shifts are −9, −12, and −6 cm^{-1}. According to the calculations, the intermediate wavenumber range is found to originate from molecules coordinated from one end within the cluster. The computational evaluation sets the lower bound to $n = 5$ for clusters to exhibit wavenumbers that begin to overlap with the bulk doublet. The pentamer already shows the structural motif of solid iodine, which explains the resemblance of the spectrum to that of the bulk. The $n = 7$ case results can be interpreted with a language adopted from either the molecular or the bulk points of view. The annealing of the dilute I_2:Kr samples reveals a sharp onset of molecular mobilization at 52 K resulting in a loss of the signal from the small aggregates and a rise of the crystalline phase doublet. Together with the observation that a large amount of the cohesion energy is reached already by a small planar slab of a crystal, iodine shows a fast transition from the isolated molecule limit to the mesoscopic scale in terms of the structure and vibrational spectrum.

Acknowledgment. Financial support is based on Academy of Finland decision nos. 124974 and 122620. CSC, the Finnish IT center for science, is acknowledged for the computational resources.

Supporting Information Available: Expanded computational evaluation of the cluster structures and spectra using ab initio and DFT methods. Discussion of the evaluation results, appropriate references, tabulations of formation energies, representative distances, vibrational wavenumbers, and cluster *Z*-matrices. The calculated Raman cross sections, polarizability derivatives, and IR intensities for monomer, dimer, pentamer, and heptamer modes. This material is available free of charge via the Internet at http://pubs.acs.org.

JA806537U